Vibrational dynamics of a stepped metallic surface: Step-edge phonons and terrace softening on Ni(977)

L. Niu,[a] D. D. Koleske,[b),c)] D. J. Gaspar,[b)] and S. J. Sibener[b)]
The James Franck Institute, The University of Chicago, Chicago, Illinois 60637

(Received 30 December 1994; accepted 7 March 1995)

Inelastic helium atom scattering has been used to measure the surface and step localized phonons on a stepped metallic surface, Ni(977). These time-of-flight measurements were carried out both perpendicular and parallel to the step direction. Surface phonon dispersion data collected across the steps show backfolding of the surface Rayleigh mode, and, most importantly, dramatic softening as compared to the forces present at the smooth Ni(111) surface. This softening suggests significant relaxation perpendicular to the step edge. Single-phonon scattering data collected along the step direction reveals the presence of two new step-edge localized modes, as well as the Rayleigh mode for this direction of the crystal. The Rayleigh mode here does not exhibit the notable softening that was found for the other direction. Novel in- and out-of-phase scattering measurements, with respect to the terraces, lead us to assign the new step induced modes as the two transversely polarized vibrations which propagate along the direction of the step edge. An analytic one-dimensional lattice model is proposed which well represents the dispersion data for these two step modes; its use allows us to determine the effective local force field in the two transverse directions with respect to the step edge. The findings reported herein shed new light on such topics as interface stability, crystal growth, and charge redistribution in the vicinity of well-characterized extended surface defects. © *1995 American Institute of Physics.*

I. INTRODUCTION

Steps belong to a generic defect class, line defects. They are of great interest because of their fundamental and technological importance in atomic-level interfacial phenomena. Steps themselves can be viewed as quasi-one-dimensional systems where novel physics can be explored. Steps are also known to play an important, and at times controlling, role in determining the pathways and reaction rates for heterogeneous processes such as chemical catalysis and corrosion.[1–4] Moreover, steps are common topological features during crystal growth; therefore the stabilities of steps on clean interfaces, as well as in the presence of foreign adsorbates, have to be well understood. How their presence modifies the forces and stress-fields present at interfaces with respect to those of a perfectly smooth crystalline interface is particularly central to an improved understanding of crystal growth and interface stability.[5–13] Steps also play an important role in critical behavior at phase transitions.[14,15] For all of these reasons, it is important to understand the basic properties of steps: structural, vibrational, and electronic.

Phonon (vibrational) measurements directly provide information on interatomic forces. The frequency and dispersion of various modes can give important bonding information; for instance, the surface Rayleigh mode supplies information about the relaxation of the topmost surface layer with respect to the bulk. Here we will focus on the properties of vicinal surfaces, i.e., ones which contain a significant population of well-defined atomic-level steps, as they provide a nearly ideal model system for examining the properties of extended surface defects. The measurement of phonons on stepped surfaces can conceptually be divided into two categories; (i) the study of step localized phonons, which provide information on local forces at steps, and (ii) surface phonon measurements which yield information about the effect of steps on the neighboring terrace atoms. Such measurements nicely complement low energy electron diffraction (LEED) studies and *ab initio* calculations which have examined structural relaxations caused by the presence of steps, with the driving force being electronic charge smoothing near steps.[16,17] Further, the observation of step localized phonon modes is the first evidence of collective vibrations of a one-dimensional lattice;[18] they also give information on a more fundamental level of how steps, which break the local translational symmetry of an otherwise perfect atomic environment, affect interatomic forces.

There has been some theoretical work on the vibrations of stepped surfaces.[19–24] Knipp[20,21] performed extensive calculations of step phonons, with detailed analysis of the polarization of these modes. His results show that step phonons have polarizations similar to those of the surface phonons of the step face near the surface Brillouin zone (SBZ) boundary. Berndt *et al.*[22] also examined step-edge induced modes, predicting the presence of two new resonant optical modes, and again describing their polarizations at the SBZ boundary. In other work, Koleske[24] calculated spectral densities for phonon modes on a variety of stepped surfaces, predicting once again the existence of step localized phonons. Of particular relevance to this study was the suggestion by both Berndt *et al.* and Koleske that a vicinal metal (111) surface having a (100) step face would be an excellent candidate for inelastic helium atom scattering experiments of step-edge phonon dynamics. The few experiments done so far[25–27] show new modes at or near the SBZ center. Inelastic electron scattering

[a)]Also Department of Physics, The University of Chicago.
[b)]Also Department of Chemistry, The University of Chicago.
[c)]Current address: Naval Research Laboratory, Washington, DC 20375.

Downloaded 14 Sep 2004 to 143.106.6.126. Redistribution subject to AIP license or copyright, see http://jcp.aip.org/jcp/copyright.jsp

(HREELS) measurements by Ibach *et al.*[25] show one step phonon at the SBZ center for a Pt(775) surface. Wuttig and co-workers,[26] also using HREELS, were only able to observe the backfolding of the surface phonon mode for TiC(310) due to the change of the surface periodicity caused by steps. Lock *et al.*[27] measured one step induced phonon branch (which they labeled as E_1) on Al(221) using helium atom scattering. A general and intuitive finding coming from the aforementioned studies is that the step induced phonon modes are only narrowly separated energetically from the surface phonons found on terraces. This necessitates the use of a high resolution probe (both energy and momentum) for studying these new phonon modes. Furthermore, because of the smaller population of steps compared to that of terraces, step sensitive probes must be used. Helium atom scattering is an ideal choice in this situation; it is surface sensitive, nondestructive, and has, in many instances, sensitivity to steps that is superior to that of electron scattering.[28] In what follows, we will show how the judicious choice of scattering conditions (in- and out-of-phase with respect to the terraces) can further enhance the utility of inelastic helium atom scattering for studying step induced phonon modes.

This study will focus exclusively on Ni(977), a vicinal surface consisting of (111) terraces and (100) step edges. Nickel is a particularly advantageous material for this investigation as its bulk phonon dispersion is well represented by a single force constant model of its dynamics.[29] Important supporting information is also readily available from previous phonon studies of the (100),[30] (110),[29] and (111)[31] surfaces of nickel.

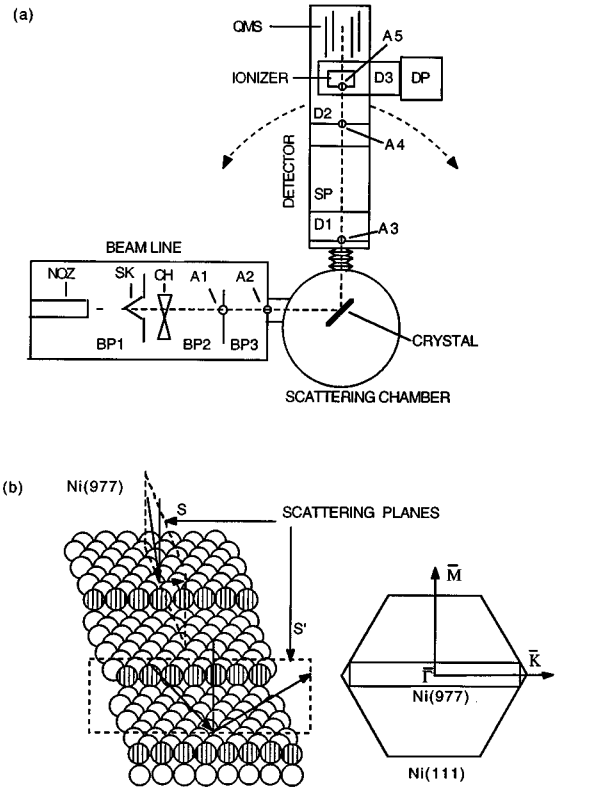

FIG. 1. Schematic view of our helium scattering machine is shown in (a). It consists of three parts; beamline, scattering chamber, and detector. Our sample Ni(977) is illustrated in (b) where the two scattering planes are also designated. Also shown is the first surface Brillouin zone (SBZ) of Ni(977) enclosed by that of Ni(111).

II. EXPERIMENT

Experiments were performed with a high energy and momentum resolution helium scattering instrument which has been previously described in some detail.[18,32] This low energy, neutral atom scattering instrument, shown schematically in Fig. 1(a), can be viewed as consisting of three parts; beamline, scattering chamber, and rotating quadrupole based detector. Operating parameters/instrument settings used in these experiments can be found in Tables I and II.

The supersonic atom beam source (UHP grade 99.999% helium) produces a nearly monochromatic incident flux of helium atoms (e.g., for $T_{\text{nozzle}}=112$ K; $\Delta t/t$ of 0.66%, or a Mach number of 274) and utilizes a two-stage closed-cycle helium refrigeration system in order to operate at temperatures between ~40 K and 300 K (typical nozzle temperatures used in this study covered 74 K–120 K). Different incident wave vectors are generated by temperature tuning of the nozzle tip to the desired setting; energies spanning the range 14–26 meV were used in this study. The beamline has three differential pumping regions; the first contains the nozzle-skimmer beam generation region, the next a dynamically balanced time-of-flight chopper disk (which contains multiple time-of-flight, diffraction, and cross-correlation modulation patterns; conventional single-shot time-of-flight pulses were used in these studies), and the third acts as a buffer pumping chamber before the beam enters the scattering chamber. The scattering chamber is pumped by ion, Ti sublimation, and cryogenically baffled diffusion pumps. Added pumping speed comes from a two-stage closed cycle helium refrigerator which we use for cooling the target assembly. Base pressures of $\sim 7\times10^{-11}$ Torr are routinely achieved. The Ni sample is mounted on a manipulator which allows for adjustment of the crucial degrees of freedom; sample *XYZ* translation, as well as tilt, azimuth, and polar angles. The manipulator rides on a large triply differentially sealed rotating lid

TABLE I. Typical experimental parameters.

Helium grade	99.999%
Nozzle diameter	25 μ ($\pm$2.5 μ)
Nozzle stagnation pressure	600–750 psi
Nozzle temperature	74–120 K
Incident beam energy	~14–26 meV
Incident de Broglie wavelength	~0.87–1.2 Å
Incident wave vector	~5.2–7.2 Å^{-1}
Mach number	~270
Relative velocity spread ($\Delta v/v$)	~0.66%
Chopper wheel frequency	~125–200 Hz
Chopper gate width	8–14 μs
TOF channel width	4 μs
TOF channel number	255
Ionizer length (geometric)	~0.9 cm
Energy resolution	0.46 meV
Angular resolution	0.36° FWHM
Background counting rate (detector closed)	20 Hz
Background counting rate (detector open/TOF)	30 Hz

Downloaded¬14¬Sep¬2004¬to¬143.106.6.126.¬Redistribution¬subject¬to¬AIP¬license¬or¬copyright,¬see¬http://jcp.aip.org/jcp/copyright.jsp

TABLE II. Aperture system dimensions.

	Distance from nozzle (cm)[a]	Aperture size (cm)	Angle from nozzle (deg)[b,c]
Nozzle	0.00		
Skimmer	0.07–0.22	0.05	
Chopper	13.5	0.05	
Aperture 1	16.1	0.089	0.32
Aperture 2	35.8	0.193	0.31
Crystal	68.5		
Aperture 3	94.6	0.445	0.27(0.98)
Aperture 4	158.1	0.556	0.20(0.36)
Aperture 5	165.6	0.579	0.20(0.34)
Ionizer plate	168.9	0.635	0.22(0.36)
Ionizer filament	170.0		

[a]The distances in column two are for the long machine configuration. The path length can be shortened by removing the 44.45 cm spacer between apertures 3 and 4.

[b]The numbers in column four refer to the distance from the nozzle. The angle subtended from the *crystal* by the detector apertures are in parentheses. All numbers refer to the long machine configuration. For the shortened machine, the values corresponding to apertures 4, 5, and the ionizer plate would be 0.28°(0.71°), 0.27°(0.63°), and 0.29°(0.65°).

[c]The beam spot size on the crystal is estimated to be 3.7 mm for normal incidence.

(spring-loaded Teflon gaskets) and is mounted 5.08 cm from the center of flange rotation. This allows the sample to be placed into a variety of positions in the scattering chamber such as the scattering center of the instrument, sputtering, LEED, Auger, etc. Finally, the detector consists of three differentially pumped regions which rotate, under computer control, by ±20° around the scattering center. This arrangement we view as ideal, as it permits data to be obtained at a variety of final scattering angles while using fixed incident kinematic conditions. It is especially advantageous when comparing the data to quantum scattering conditions (one calculation gives all final states); it also avoids the problem of large changes in scattering cross sections coming from incident-state selective adsorption resonances. The actual detector consists of an electron ionizer/quadrupole mass spectrometer (the ionizer separately nested in a turbomolecular-pumped region which is in turn backed by a diffusion pump to achieve higher helium compression before being evacuated by a mechanical pump). The entire detector assembly is mounted on an optical rail support system which permits change of the flight path between the crystal and the ionizer. In these studies we used the highest resolution ''long flight path'' setting; chopper-to-crystal distance 55.1 cm and crystal-to-ionizer distance 101.5 cm. The composite energy and angular resolution parameters for the instrument as configured for these experiments were 0.46 meV and 0.36° (corresponding to a momentum resolution of 0.038 Å^{-1}), respectively.

The surface we studied was Ni(977), provided by Princeton Scientific Corp. It was prepared by cutting a Ni single crystal 7.02° away from the (111) plane along the (211) direction. The crystal orientation was verified to be within 0.5° of the ideal (977) direction with Laue x-ray back-reflection. The surface can also be labeled as Ni[8(111)×(100)] in microfacet notation,[33] which indicates that the surface consists of (111) terraces that are 8 atomic rows wide and (ideally) straight (100) steps that are one atom high, Fig. 1(b). The crystal was cleaned by Ar^+ sputtering during repetitive temperature cycles (between 400 K and 1100 K) and then annealed at 1100 K. Surface order was checked by LEED, and surface cleanliness by Auger spectroscopy. The major contaminant in this crystal was sulfur. The sulfur peak at 152 eV was finally reduced to less than 0.1% of the Ni peak at 62 eV, which was the limit of our Auger sensitivity.

Dispersion curves are calculated by assuming single phonon interactions and using the conservation of surface parallel momentum and total energy

$$\mathbf{K}_f = \mathbf{K}_i + \mathbf{G} + \mathbf{Q}, \tag{1}$$

$$\mathbf{k}_f^2 = \mathbf{k}_i^2 + \frac{2m}{\hbar^2}\,\Delta E(\mathbf{Q}), \tag{2}$$

where $\mathbf{K}_i$ and $\mathbf{K}_f$ are the surface projections of the helium atom's incident and final wave vectors, $\mathbf{k}_i$ and $\mathbf{k}_f$ (i.e., $|\mathbf{K}_i| = |\mathbf{k}_i| \sin\theta_i$ and $|\mathbf{K}_f| = |\mathbf{k}_f| \sin\theta_f$, where θ_i and θ_f are the incident and final angle of scattering with respect to the surface normal). $\mathbf{G}$ is the surface reciprocal lattice vector, $\mathbf{Q}$ is the momentum transfer, and $\Delta E(\mathbf{Q})$ is the energy transfer. From Eqs. (1) and (2), we have

$$\Delta E(\mathbf{Q}) = \frac{\hbar^2}{2m}\left[\left(\frac{k_i \sin\theta_i + \Delta K}{\sin\theta_f}\right)^2 - \mathbf{k}_i^2\right], \tag{3}$$

where $k_i = |\mathbf{k}_i|$ and $\Delta K = \pm|\mathbf{G}+\mathbf{Q}|$. The + and − signs refer to the direction of $\mathbf{G}+\mathbf{Q}$ with respect to $\mathbf{K}_i$. This relationship between ΔE and ΔK defines what are called scan curves, the locus of energy and momentum acceptance conditions for given incident and final scattering parameters. For single phonon interactions, points where the scan curves intersect phonon dispersion curves correspond to possible quantum transitions

$$\Delta E(\mathbf{Q}) = \pm\hbar\omega(\mathbf{Q}). \tag{4}$$

The (+) sign refers to phonon annihilation, and the (−) sign to phonon creation.

By measuring the final velocity of the scattered helium atom at a well-defined angle, we can determine both the phonon momentum and energy. Measuring these quantities over a range of angles, we can map the phonon dispersion curve.

Two scattering directions were chosen for the experiments [Fig. 1(b)]. One had the sagittal plane perpendicular to the steps [labeled as S in Fig. 1(b)], the other had the sagittal plane parallel to the steps and perpendicular to the terraces, i.e., the terrace normal was included in the scattering plane [labeled as S' in Fig. 1(b)]. The crystal orientation was characterized by in-plane scattering of the helium atom beam from the stepped surface, as well as He–Ne laser reflections and LEED. Only in-plane scattering data were collected, defined as the plane which included the incident beam, the surface normal, and the plane of detector rotation.

Throughout these measurements, we made judicious use of in-phase and out-of-phase scattering conditions to pick up phonon modes of different symmetries and different polarizations. The in-phase condition, which corresponds to con-

Downloaded¬14¬Sep¬2004¬to¬143.106.6.126.¬Redistribution¬subject¬to¬AIP¬license¬or¬copyright,¬see¬http://jcp.aip.org/jcp/copyright.jsp

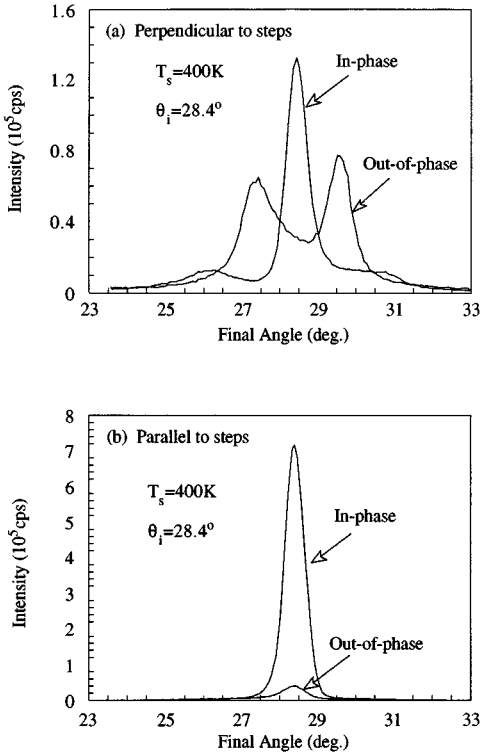

FIG. 2. Comparison of diffraction spectra for in-phase and out-of-phase scattering from the clean single stepped surface. Panel (a) has the scattering plane perpendicular to the steps. The single peak was obtained using in-phase conditions and the double peak using out-of-phase conditions. Panel (b) has the scattering plane parallel to the steps and perpendicular to the terraces. The high signal peak was obtained using in-phase conditions and the low signal peak using out-of-phase conditions.

structive interference between the atom beams specularly scattered ($\theta_i = \theta_f$) from adjacent terraces, satisfies

$$kh(\cos\ \theta_i + \cos\ \theta_f) = 2kh\ \cos\ \theta_i = 2n\pi, \tag{5}$$

when n is an integer, k is the incident momentum, h is the step height in the direction of the terrace normal, and θ_i (θ_f) is the incident angle (final angle) with respect to the terrace normal. Similarly, the out-of-phase condition, which corresponds to destructive interference between the atom beams specularly scattered from adjacent terraces, satisfies

$$kh(\cos\ \theta_i + \cos\ \theta_f) = 2kh\ \cos\ \theta_i = (2n+1)\pi. \tag{6}$$

Figure 2 shows diffraction spectra under in-phase and out-of-phase conditions. The spectra in the upper panel were taken with the sagittal plane perpendicular to the steps, while the spectra in the lower panel were taken with the sagittal plane parallel to the steps. Both geometries reveal (the expected) dramatic changes in scattering behavior as we switch from in- to out-of-phase kinematics; across the steps we see a transformation from two to one diffraction peaks, while along the steps we see a specular intensity change of nearly two orders of magnitude. The consequences of collecting data with such carefully selected conditions will be fully discussed in the next section of this paper.

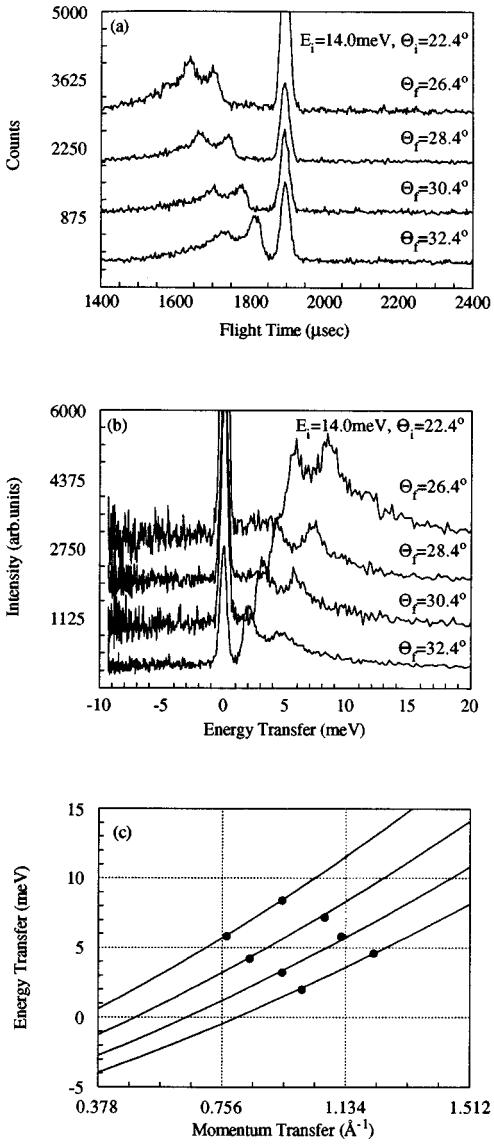

FIG. 3. The surface Rayleigh mode measured using in-phase conditions in the scattering plane perpendicular to the steps. Panel (a) shows a typical group of time-of-flight spectra. Panel (b) shows the same data with time converted to energy transfer. Panel (c) shows the data plotted as energy transfer vs momentum exchange. The solid lines are the scan curves.

III. RESULTS

A. Surface phonons

Let us first look at the measurements made with the scattering plane perpendicular to the steps. These spectra were taken with the beam scattering in-phase, with an incident energy of 14.0 meV and an incident angle Θ_i of 22.4°. Throughout this paper, Θ_i is the incident angle with respect to the macroscopic surface normal, and θ_i is the incident angle with respect to the terrace normal. Therefore, $\Theta_i = \theta_i - 7.02°$ for ''upstairs'' scattering, the geometry used in this study. A typical group of time-of-flight spectra, taken at different final angles, at a crystal temperature of 400 K, is shown in Fig. 3(a). Figure 3(b) shows the spectra converted to energy transfer. The two inelastic peaks are due to scatter-

Downloaded¬14¬Sep¬2004¬to¬143.106.6.126.¬Redistribution¬subject¬to¬AIP¬license¬or¬copyright,¬see¬http://jcp.aip.org/jcp/copyright.jsp

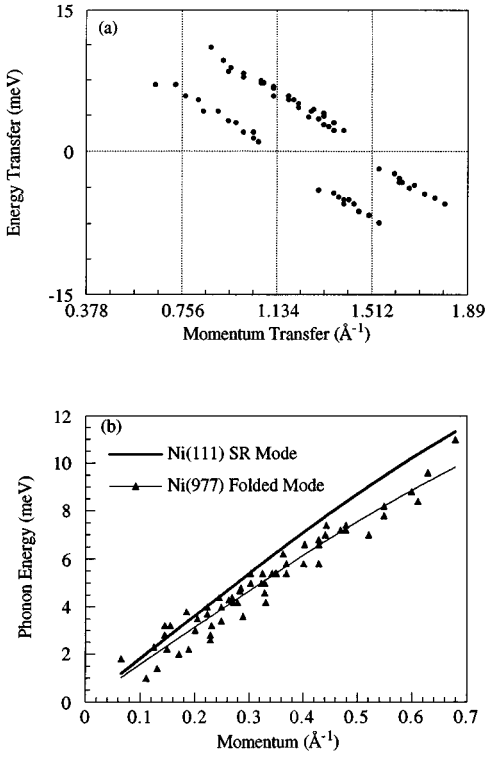

FIG. 4. All of the data taken with scattering plane perpendicular to the steps and using in-phase conditions. Panel (a) shows energy transfer vs momentum exchange and panel (b) shows the folded zone phonon dispersion curve.

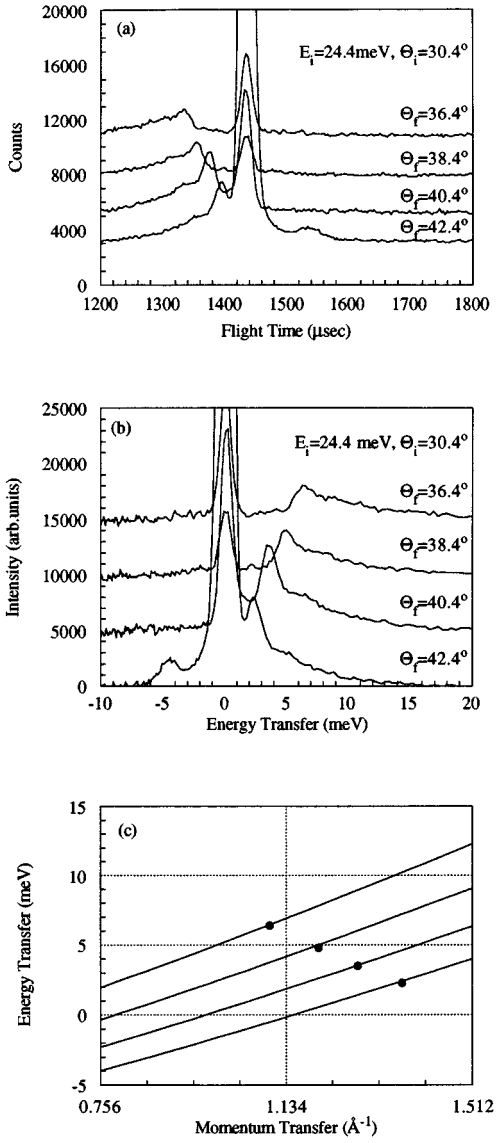

FIG. 5. The surface Rayleigh mode measured using out-of-phase conditions in the scattering plane perpendicular to the steps. Panel (a) shows a typical group of time-of-flight spectra. Panel (b) shows the same data with time converted to energy transfer. Panel (c) shows the data plotted as energy transfer vs momentum exchange. The solid lines are the scan curves. The other (apparent) inelastic feature in the lowest spectrum is actually an artifact, called a decepton, which is actually diffracted elastic flux coming from the finite energy spread of the incident helium beam.

ing from the surface Rayleigh mode. Surface Rayleigh mode folding is clearly illustrated by Figs. 3(c) and 4(a). Figure 3 shows the intersection of the relevant scan curves with the data, while Fig. 4(a) clearly shows that the two observed ''folded'' phonon branches are related by a simple linear translation in momentum space by 0.378 Å^{-1} along the momentum transfer axis. This mode folding is due to the new periodicity created by steps and can be understood as the modulation of (111) surface along the ΓM direction by the steps. The new periodicity in real space is 16.65 Å. In reciprocal space, this is $(2\pi/16.65)=0.377$ Å^{-1}, equal to 0.378 Å^{-1} within experimental uncertainty.

Figure 4(b) shows all the data points folded back into the first SBZ. The Ni(111) surface Rayleigh mode[31] along the ΓM direction is also shown (thick line). The thin line in Fig. 4(b) is a sine curve fit to our experimental data. *One should especially note that the Rayleigh mode of Ni(977) is appreciably softened as compared to that of the Ni(111) surface.*

Additional data across the steps was taken using out-of-phase conditions (the incident helium beam energy was 24.4 meV and the incident angle Θ_i was 30.4°). Figure 5 shows a sampling of such time-of-flight spectra and their respective energy transfer spectra for 400 K surface. Folding of the surface Rayleigh mode is not expected to be seen under these conditions since He scattered from adjacent terraces interfere destructively, resulting in the loss of sensitivity to the additional periodicity imposed by the steps. Indeed, mode folding was not experimentally observed as shown in Fig. 6(a). The surface Rayleigh mode, now only a single peak, was better resolved. Thus the data are much less noisy, and the surface Rayleigh mode softening on Ni(977) in comparison with Ni(111) is clearly demonstrated, Fig. 6(b). Fitting the Rayleigh mode of both the in-phase and out-of-phase data gives maximum phonon energies at the M SBZ boundary of 14.8 and 15.0 meV, respectively. These two numbers agree within experimental error, and are much softened as compared to Rayleigh mode of the Ni(111) surface, which has a maximum zone edge energy of 17.2 meV.[31] The softening of the force constant as compared to the bulk value is calculated to be 32%, which is much bigger than the 11% softening previously seen by our group for the Ni(111) surface.[31] One plausible explanation would be that the eight rows of terrace atoms relax from their corresponding equilibrium positions

Downloaded¬14¬Sep¬2004¬to¬143.106.6.126.¬Redistribution¬subject¬to¬AIP¬license¬or¬copyright,¬see¬http://jcp.aip.org/jcp/copyright.jsp

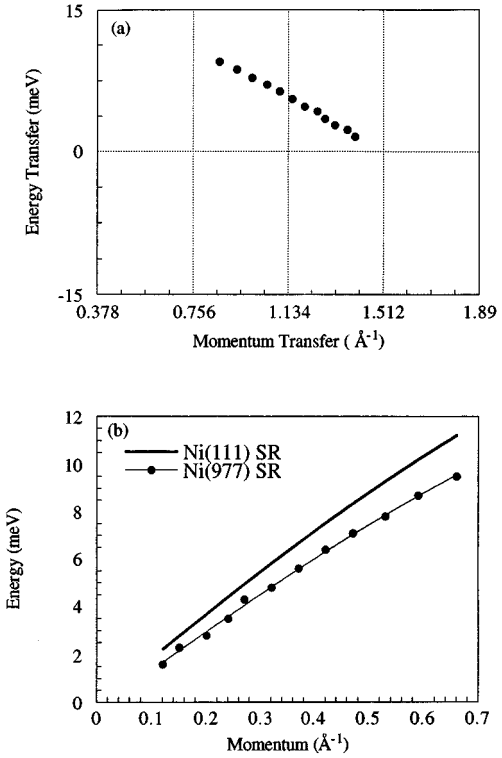

FIG. 6. All of the data taken with scattering plane perpendicular to the steps and using out-of-phase conditions. Panel (a) shows energy transfer vs momentum exchange and panel (b) shows the folded zone phonon dispersion curve.

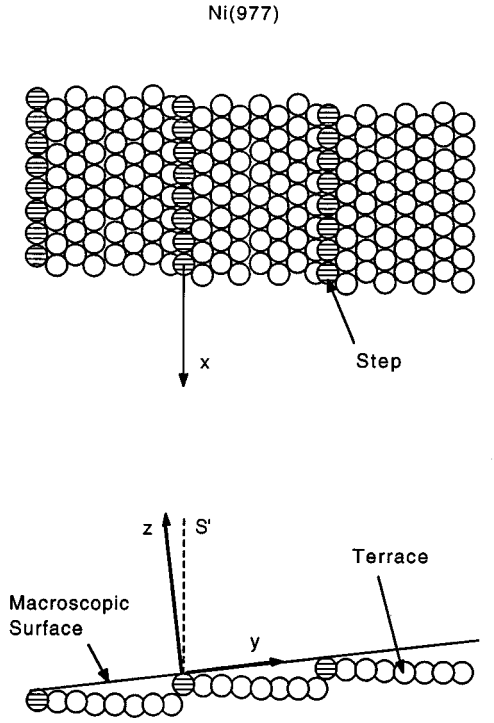

FIG. 8. The Ni(977) surface and polarization directions for the step localized phonon modes.

on the (111) surface, similar to Al(331),[16,17] where oscillatory relaxations up to 11.7% were observed. Another reason might be the effect of charge smoothing[17] near steps. Finite size effects[17] could also be a factor; the size of the surface for collective vibration is effectively eight rows of atoms. A realistic *ab initio* calculation is needed for Ni(977) to determine the various contributions to the observed softening.

Is the surface Rayleigh mode in the other direction (parallel to steps) softened? Figure 7 shows the result measured in the scattering plane parallel to the steps under in-phase and out-of-phase conditions. Clearly no surface Rayleigh mode softening is observed as compared to Ni(111) along the $\bar{\Gamma}\bar{K}$ direction.[34] The mode is not softened because, parallel to the steps, the terraces are undisturbed.

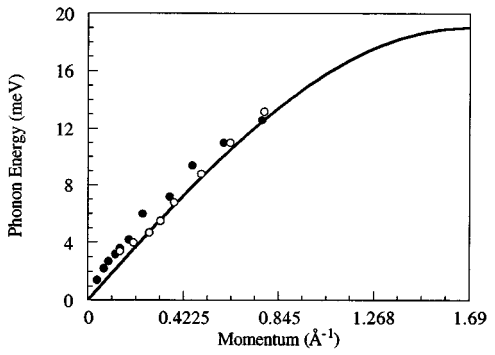

FIG. 7. The surface Rayleigh mode measured using in-phase (filled circles) and out-of-phase (open circles) conditions in the scattering plane parallel to the steps and perpendicular to the terraces.

B. Step localized phonons

Step induced phonons are the phonons which are essentially localized to, and propagating along, the steps.[18] What are the possible normal modes for step localized phonons? A simplified answer comes from considering a step row of atoms as a one-dimensional lattice oriented and in contact with a three-dimensional lattice, similar to phonons propagating along high symmetry directions in cubic crystals.[35–37] Based on this model, there is a longitudinal mode polarized along, and two transverse modes polarized perpendicularly to, the steps. Consider the symmetry of this row of atoms (Fig. 8). One of the symmetry directions (the *y* direction) is along the macroscopic surface and perpendicular to the steps, where there is translational symmetry. The other symmetry direction (the *z* direction) is the normal to the macroscopic surface. These are the possible polarizations of the two transverse modes.

In order to detect step induced phonons which propagate along the steps, the scattering plane has to be chosen parallel to them. Helium atom scattering is mainly sensitive to the variation of the He-surface interaction potential perpendicular to the surface. A surface lattice vibration will strongly couple with the He beam if the displacement vector of the vibration has an appreciable projection onto the surface normal. For a one-dimensional lattice, the polarization falls in the same direction as the displacement. Helium scattering

Downloaded¬14¬Sep¬2004¬to¬143.106.6.126.¬Redistribution¬subject¬to¬AIP¬license¬or¬copyright,¬see¬http://jcp.aip.org/jcp/copyright.jsp

therefore will primarily couple to phonon polarizations which have projections onto the surface normal. Then how do we choose the scattering plane? We know that it must be parallel to the steps. One easy choice would be the scattering plane perpendicular to the macroscopic surface, but only the *z* polarization would be detected since the scattering plane would be perpendicular to the *y* polarization. It is also difficult to determine when the scattering plane is precisely aligned to the macroscopic surface normal since in-plane scattering of the He atoms cannot be used, and He–Ne laser reflection is not sufficiently accurate. One can choose the scattering plane to be perpendicular to the terraces as shown by S' in Fig. 8. Because the scattering plane is perpendicular to the terraces, the in-plane scattering of helium atoms can be used to determine the crystal orientation precisely. Notice also that both *y* and *z* polarizations have projections on the scattering plane, thus both modes can be observed under this condition. We therefore adopted this geometry for our step phonon measurements.

Can we use in-phase and out-of-phase conditions to detect the two polarizations separately (and in fact to assign the polarizations of the observed phonon modes)? The answer is yes. The phonon mode that is most sensitive to in- or out-of-phase conditions is *z*-polarized; it is only 7° from the terrace normal. Using in-phase conditions, inelastic scattering arising from the *z*-polarized phonon mode will be enhanced due to constructive interference effects which influence both the elastic and inelastic cross sections. This interference becomes destructive when out-of-phase conditions are used. This effect is much less pronounced for the *y*-polarized mode. Therefore, under in-phase conditions, the *z*-polarized phonon mode is observed and the *y*-polarized phonon mode signal is not strong enough to be detected. With out-of-phase conditions, the *z*-polarized phonon mode signal is effectively nulled and the *y*-polarized phonon mode is observed, a predominantly shear horizontal mode that can be detected because of the broken mirror reflection symmetry with respect to the scattering plane. The surface Rayleigh mode is observed at all times due to the large number of terrace atoms. (One should also note before proceeding that the polarizations of the step-induced modes in reality are not purely linearly polarized throughout the SBZ; nevertheless, as seen below, the above arguments for a perfect one-dimensional lattice chain capture the essential physical behavior of the two new step-induced phonon modes near Γ, the center of the SBZ.)

Figure 9(a) shows typical time-of-flight spectra taken with in-phase conditions. For these runs the incident helium beam energy was 17.9 meV, the incident angle was $\theta_i = 37.4°$, and the crystal temperature was 300 K. Figure 9(b) shows these spectra converted to energy transfer, followed by the dispersion curves[34] and corresponding scan curves in Fig. 9(c). Clearly, there are two inelastic features, one due to the Rayleigh mode, and one (E_1) unique to this stepped surface.

Figure 10(a) shows typical time-of-flight spectra taken with out-of-phase conditions. Here the incident helium beam energy was 24.4 meV, the incident angle was $\theta_i = 37.4°$, and the crystal temperature was 250 K. Figure 10(b) shows these

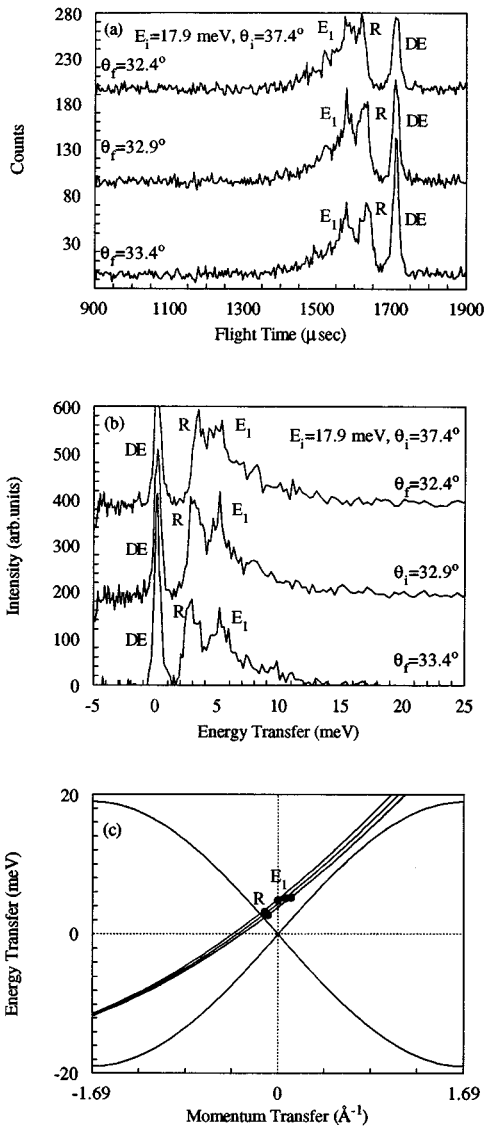

FIG. 9. A typical group of time-of-flight spectra taken with the scattering plane parallel to the steps and using in-phase conditions, their energy transfer spectra, and the corresponding energy transfer vs momentum exchange. DE denotes the diffuse elastic peak, *R* is for inelastic scattering from surface Rayleigh mode, and E_1 for inelastic scattering from the new mode. The solid lines through *R* and E_1 in (c) are the scan curves. The remaining solid lines in (c) is the calculated Ni(111) surface Rayleigh mode using the simple sine function, scaled using the maximum energy at *K* point (19.0 meV) measured by Stirniman *et al.* with inelastic electron scattering.

spectra converted to energy transfer, followed by the dispersion curve and corresponding scan curves in Fig. 10(c). Again, there is an inelastic feature (E_2) unique to this stepped surface, as well as the Rayleigh wave.

Figure 11 shows the dispersion curves generated from all of the time-of-flight data. Note that E_1 and E_2 do not belong to the same phonon dispersion branch, which agrees with our simplified view of step induced phonons. Following our expectations, E_1 is observed using in-phase conditions because of its *z* polarization, while E_2 is observed using out-of-phase conditions because of its *y* polarization. The longitudinal

Downloaded¬14¬Sep¬2004¬to¬143.106.6.126.¬Redistribution¬subject¬to¬AIP¬license¬or¬copyright,¬see¬http://jcp.aip.org/jcp/copyright.jsp

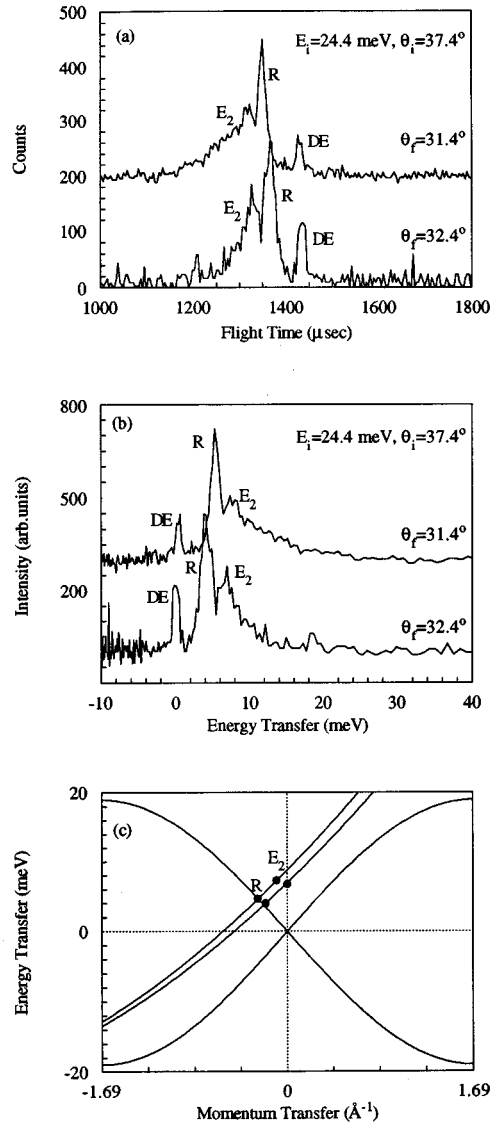

FIG. 10. A typical pair of time-of-flight spectra taken with the scattering plane parallel to the steps and using out-of-phase conditions, their energy transfer spectra, and the corresponding energy transfer vs momentum exchange. E_2 is the other new mode. The solid lines through R and E_2 in (c) are the scan curves. The remaining solid lines in (c) is the calculated Ni(111) surface Rayleigh mode using the simple sine function, scaled using the maximum energy at K point (19.0 meV) measured by Stirniman *et al.* with inelastic electron scattering.

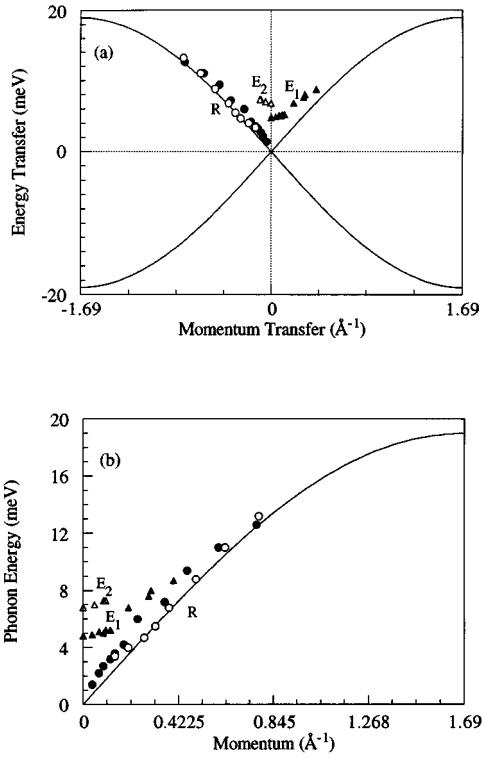

FIG. 11. Panel (a) shows energy transfer vs momentum transfer for the E_1, E_2, and Rayleigh modes. The solid lines are the surface Rayleigh mode of Ni(111) in the ΓK direction (see Fig. 9 or 10 for details). Open symbols are for data taken using in-phase conditions, filled symbols for data taken using out-of-phase conditions. Circles correspond to the Rayleigh mode, triangles to the new modes. Panel (b) shows the same data folded into the first SBZ.

mode of the step is not observed, which may indicate its near degeneracy with the surface Rayleigh mode.

We used two methods to characterize the nature of the localization of the two new step modes. The first method was to introduce a small amount of oxygen which causes a transition from single to double steps (step doubling).[38] We have also shown[38] that oxygen moves to the step edges upon adsorption at low coverages. Therefore it is a quite reasonable expectation that such O adsorption should significantly modify the step-edge related modes as compared to the effect on the terrace-related Rayleigh wave. Figures 12(a) and 12(b) show spectra, taken using in-phase conditions, which demonstrate the effect of oxygen adsorption on E_1. An oxygen exposure of 0.048 L quenches the E_1 mode completely while the surface Rayleigh mode persists. Figures 12(c) and 12(d) show spectra taken using out-of-phase conditions. Similarly, 0.048 L of oxygen exposure is found to completely quench the E_2 mode, leaving the Rayleigh mode largely unchanged. These observations confirm our assignment of E_1 and E_2 as step-edge induced phonon modes.

We also observed that even under ultrahigh vacuum conditions (8×10^{-11} Torr), adsorption of background gases can quench the new modes. At 250 K, E_2 disappeared 20 min after the crystal was cleaned. At 300 K, E_1 disappeared 35 min after the crystal was cleaned. For both cases, the Rayleigh mode persisted. A similar sensitivity of step localized modes to impurities was also reported by Ibach *et al.*[25]

The sensitivity of the step induced modes to surface temperature has also been examined. In work reported elsewhere[39] we have assessed the structural changes which occur as a function of surface temperature. We have found sensitivity to two types of roughening; kink formation in the step row, and disordering of the rows neighboring the steps. Kink formation in the row of step atoms has a characteristic onset temperature of 300 K, while disordering of the nearest neighbor rows has a characteristic onset temperature of 550 K.[39] Figure 13 shows time-of-flight spectra measured at different crystal temperatures for both in-phase [Fig. 13(a)] and out-of-phase [Fig. 13(b)] conditions. Using in-phase conditions, E_1 persists until the crystal temperature exceeds 550

Downloaded¬14¬Sep¬2004¬to¬143.106.6.126.¬Redistribution¬subject¬to¬AIP¬license¬or¬copyright,¬see¬http://jcp.aip.org/jcp/copyright.jsp

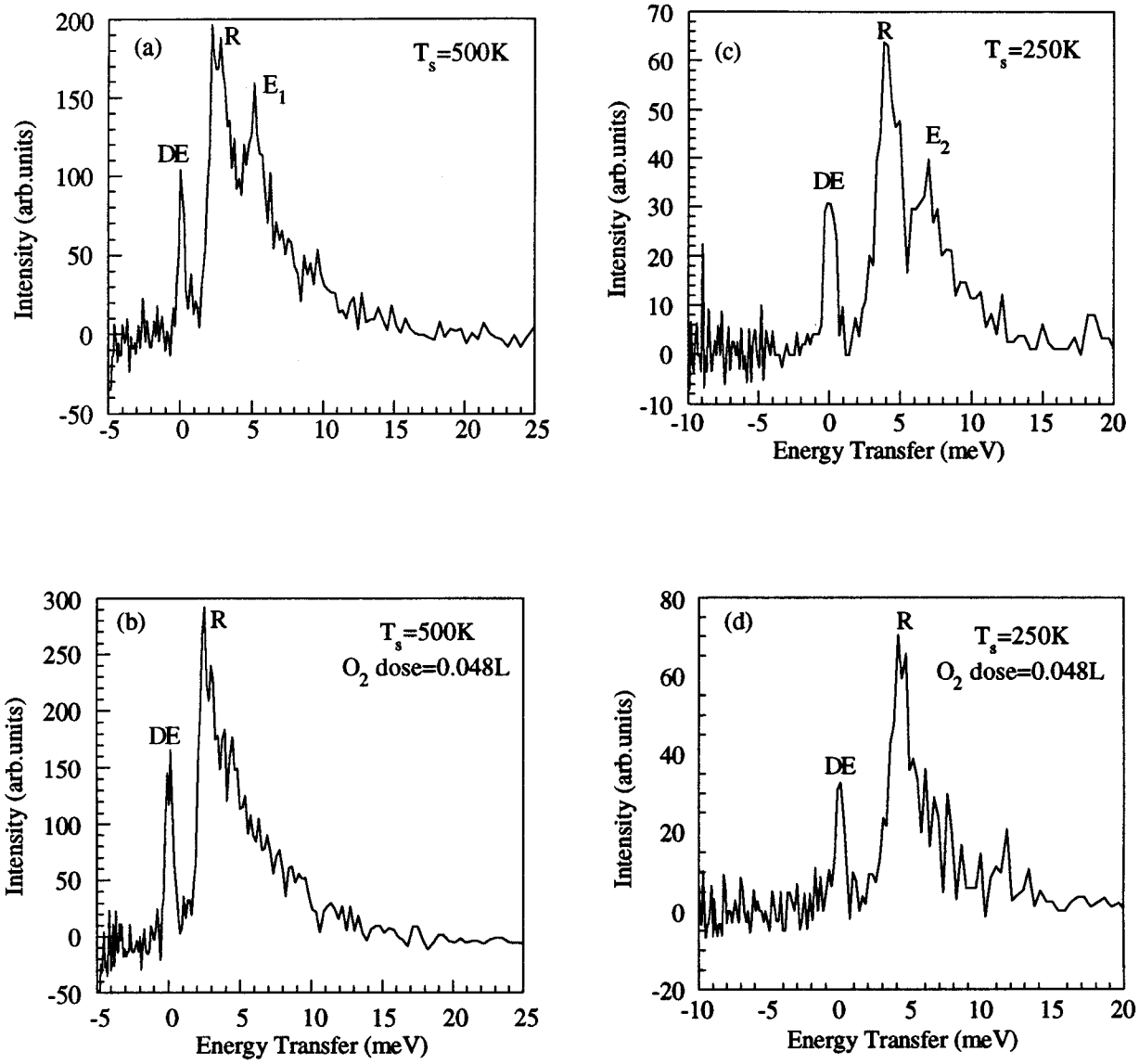

FIG. 12. Adsorbate effects on the two new modes. The left-hand side is in-phase data. Panel (a) is the spectrum for the clean crystal at 500 K. Panel (b) is the spectrum for the 500 K crystal with 0.048 L of oxygen exposure. It is clear that the new mode E_1 disappears upon oxygen dosing. The right-hand side is out-of-phase data. Panel (c) is the spectrum for the clean crystal at 250 K. Panel (d) is the spectrum for the 250 K crystal with 0.048 L of oxygen exposure. The new mode E_2 disappears upon oxygen dosing.

K. This suggests that the E_1 mode involves both the step row and its nearest neighbor rows, so it is not quenched until both are disordered. Using out-of-phase conditions, E_2 disappears when the crystal temperature is 300 K or higher, implying that E_2 is localized at the step row only, so that the roughening of the step row alone (i.e., the large scale formation of kinks) quenches the E_2 mode. The surface Rayleigh mode persists above 550 K; it is largely unaffected by the roughening of the step edges. These temperature dependencies again support our contention that E_1 and E_2 are correctly characterized as step-edge induced modes, although E_2 is more localized than is E_1.

Signal intensities of two new modes at the SBZ center are comparable to that of a typical surface Rayleigh mode on the same surface, $\sim 1.5\times10^{-4}$ of the specular intensity for in-phase conditions and $\sim 1.2\times10^{-3}$ of the specular intensity for out-of-phase conditions. The widths of two new modes are about 2.5 meV, which is noticeably larger than that of the surface Rayleigh mode, 1.5 meV. This may indicate that the coherence at the steps is worse than the coherence on the terraces. This width could also be a finite size effect as discussed previously. Since these are actually resonant modes which are embedded within the surface projection of the bulk density of states, enhanced decay pathways to these states must also be considered. *Ab initio* or realistic MD calculations are needed to more fully explore this point.

C. One-dimensional lattice model

In the absence of molecular dynamics or lattice dynamics calculations for Ni(977), we propose a simple one-

Downloaded¬14¬Sep¬2004¬to¬143.106.6.126.¬Redistribution¬subject¬to¬AIP¬license¬or¬copyright,¬see¬http://jcp.aip.org/jcp/copyright.jsp

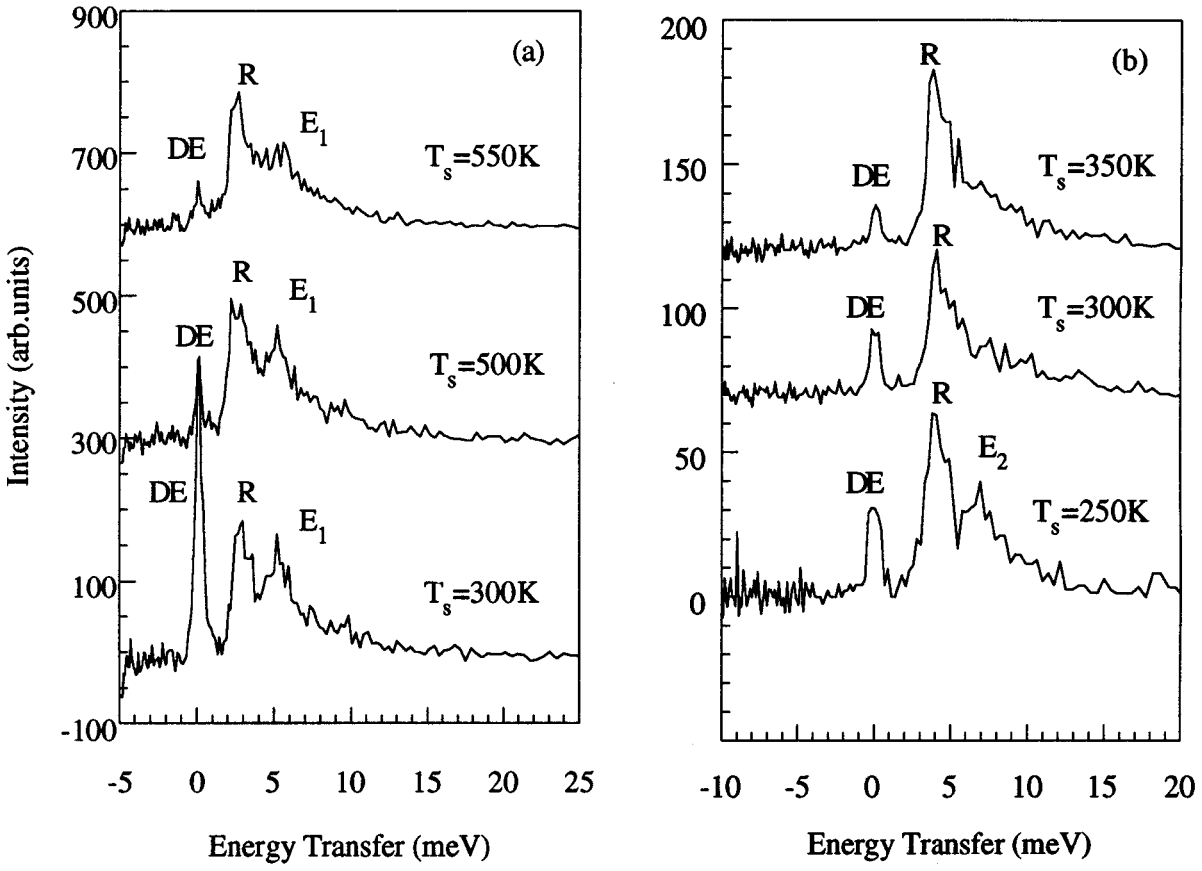

FIG. 13. The temperature dependence of the two new modes. Panel (a) is for in-phase conditions where the E_1 mode is persistent up to 500 K and is attenuated above 550 K. Panel (b) is for out-of-phase conditions where the E_2 mode starts to disappear at 300 K.

dimensional lattice model with which to analyze the step phonon data. 1D lattice models are not foreign to us. Phonons propagating along high symmetry directions in cubic crystals can be reduced to the problem of vibrations of a linear chain of atoms bounded by harmonic pair potentials.[35–37] However, we will consider a different 1D lattice model. We choose instead an highly anharmonic nearest-neighbor potential, which can be separated into an attractive part and a repulsive part. The repulsive part is a simple hard sphere potential which keeps the one-dimensional lattice from collapsing. The attractive part is responsible for the lattice vibrations. In our model, the repulsive part will be an infinite wall, and the attractive part will be approximated by springs of zero natural length and spring constant G_L [Figs. 14(a) and 14(b)]. The lattice constant is weakly temperature dependent (a_0 at $T=0$ K, and a otherwise). This chain of atoms is confined by transverse anisotropic harmonic potential well with force constants of G_1 (z direction) and G_2 (y direction), as shown in Fig. 14(c). If the deviations of the ion cores from their equilibrium positions are small, the potential of the nth atom may be approximated by nearest-neighbor interactions. Defining the small deviation along x as u, along y as v, and along z as w, the potentials may be written

$$V=\tfrac{1}{2}G_L\{(u_n+na)-[u_{n+1}+(n+1)a]\}^2+\tfrac{1}{2}G_L\{(u_n+na)-[u_{n-1}+(n-1)a]\}^2=\tfrac{1}{2}G_L(u_n-u_{n+1}-a)^2+\tfrac{1}{2}G_L(u_n-u_{n-1}+a)^2 \quad (7)$$

for the longitudinal vibrations, and

$$V=\tfrac{1}{2}G_L[(v_n-v_{n+1})^2+a^2]+\tfrac{1}{2}G_L[(v_n-v_{n-1})^2+a^2]+\tfrac{1}{2}G_2v_n^2 \quad (8)$$

for the y-polarized transverse vibrations, and

$$V=\tfrac{1}{2}G_L[(w_n-w_{n+1})^2+a^2]+\tfrac{1}{2}G_L[(w_n-w_{n-1})^2+a^2]+\tfrac{1}{2}G_1w_n^2 \quad (9)$$

for the z-polarized transverse vibrations. By solving equations of motions for three normal modes, we find for the longitudinal mode (in the x direction),

$$E_L=2\hbar\sqrt{\frac{G_L}{m}}\cdot\left|\sin\frac{1}{2}ka\right|=E_{\mathrm{lm}}\left|\sin\frac{1}{2}ka\right|. \quad (10)$$

The two transverse modes are given by

Downloaded¬14¬Sep¬2004¬to¬143.106.6.126.¬Redistribution¬subject¬to¬AIP¬license¬or¬copyright,¬see¬http://jcp.aip.org/jcp/copyright.jsp

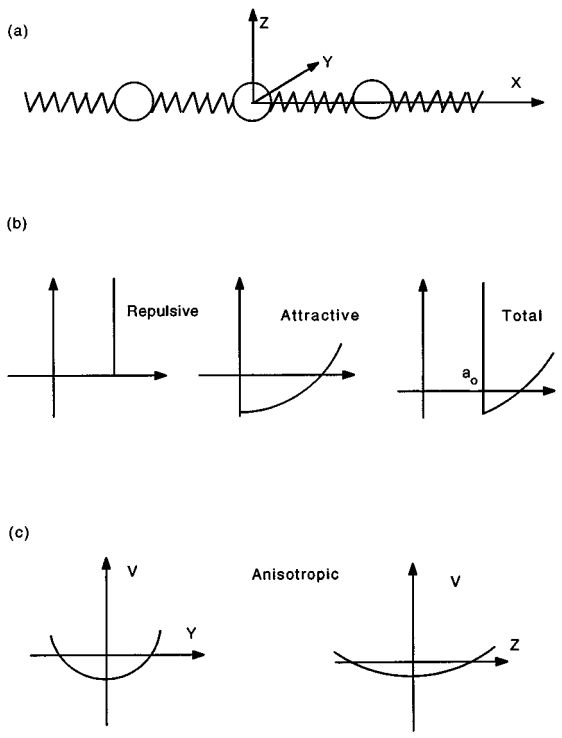

FIG. 14. (a) is the schematic of 1D lattice; (b) is the interaction potential between neighboring atoms along *x* direction; (c) is the anisotropic confining potential along *y* and *z* directions.

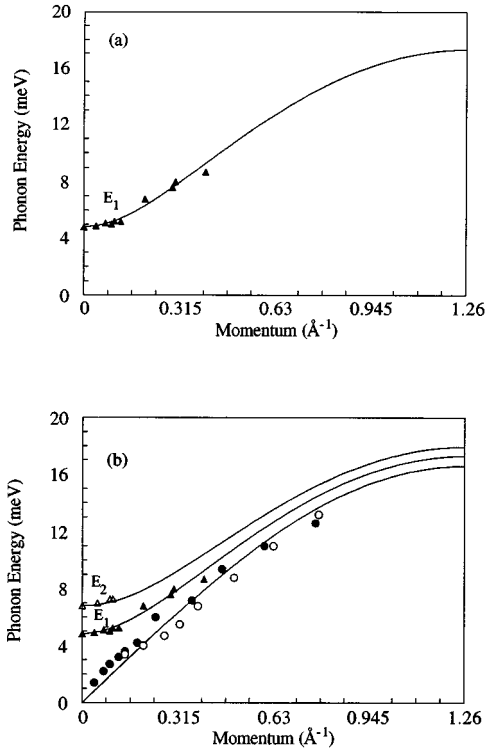

FIG. 15. Panel (a) shows the model fit to the E_1 mode. Panel (b) shows the three phonon modes of the 1D lattice confined in the 2D anisotropic harmonic potential plotted together with the experimental results.

$$E_1=\hbar\sqrt{\frac{G_1}{m}+\frac{4G_L}{m}\left(\sin\frac{1}{2}ka\right)^2}$$
$$=\sqrt{E_{10}^2+E_{\mathrm{lm}}^2\left(\sin\frac{1}{2}ka\right)^2} \tag{11}$$

in the *z* direction, and

$$E_2=\hbar\sqrt{\frac{G_2}{m}+\frac{4G_L}{m}\left(\sin\frac{1}{2}ka\right)^2}$$
$$=\sqrt{E_{20}^2+E_{\mathrm{lm}}^2\left(\sin\frac{1}{2}ka\right)^2} \tag{12}$$

in the *y* direction. E_{10} and E_{20} are the $k=0$ energies of the two transverse phonons (k is the momentum transfer), E_{lm} is the maximum energy of the longitudinal mode at the SBZ boundary, and a is the lattice constant. We choose the lattice constant of Ni, $a=2.489$ Å, as our 1D lattice constant, and $E_{10}=4.8$ meV, as measured at Γ. Fitting the data with Eq. (11) for E_1, using E_{lm} as the sole adjustable parameter, we get $E_{\mathrm{lm}}=16.2$ meV [Fig. 15(a)]. Notice that the SBZ boundaries are different in Figs. 11 and 15(a). The data were taken in the ΓK direction of Ni(111) which has a first SBZ boundary at 1.69 Å^{-1}; this is used in Fig. 11. But the real periodicity of the 1D lattice is 2.489 Å, so the 1D lattice has a first BZ boundary at 1.26 Å^{-1}, which is used in Fig. 15. The maximum energy of the longitudinal mode of the 1D lattice at X determined by the fit to be $E_{\mathrm{lm}}=16.2$ meV is quite interesting. It falls very close to the maximum energy of the surface Rayleigh mode at X for the Ni(100) surface,[30] 16.6 meV. The step faces are (100); this agreement indicates that the effective force in the direction parallel to the steps is not changed as compared to that of the ΓX direction on Ni(100). The other step localized mode can be reproduced by our model, taking $E_{20}=6.8$ meV for E_2 as determined at $\Delta K=0$, and $E_{\mathrm{lm}}=16.2$ meV, we get the fit shown in Fig. 15(b). The agreement with the experimental data are very good. Also shown in Fig. 15(b) is the dispersion relation for the longitudinal mode as determined from our model. Unfortunately, it falls very close to that of the surface Rayleigh mode, rendering it unresolvable.

The effective force constants can be calculated from the above fits; $G_1=5.2$ N/m and $G_2=10.4$ N/m. Both numbers are much smaller than the bulk single force constant of Ni, 37.9 N/m.[29] This suggests that the effective forces on the step atoms in the direction perpendicular to steps are greatly softened compared to those of the bulk or the low Miller index planes, which are softened by 10%–30% as compared to those of the bulk.[29,31] This suggests that the step atoms might be substantially relaxed from the rest of the lattice[16,17] and electronic charge redistribution might be dramatic.[17] *Ab initio* calculations on Ni(977) surface are clearly needed to explore these issues.

IV. SUMMARY AND CONCLUSION

In this paper we have presented inelastic helium scattering data which have helped delineate the dynamical properties of a stepped metallic surface, Ni(977). Several notable findings, summarized below, have come from this work deal-

Downloaded¬14¬Sep¬2004¬to¬143.106.6.126.¬Redistribution¬subject¬to¬AIP¬license¬or¬copyright,¬see¬http://jcp.aip.org/jcp/copyright.jsp

ing with step-edge induced phonon modes, as well as the extent to which the presence of steps modify the forces which govern the dynamical properties of the terraced regions of the surface. Furthermore, new scattering methodologies have been applied, based on in- and out-of-phase scattering from the terraces, which have allowed us to selectively detect and assign scattering signals arising from the two transversely polarized step-edge induced phonon branches.

When the sagittal plane was perpendicular to the steps, we only observed the surface Rayleigh mode. It exhibited unambiguous mode folding, in precise agreement with the new periodicity imposed by the Ni(977) lattice on that of Ni(111). The surface Rayleigh mode in this direction, corresponding to the $\bar{\Gamma}\bar{M}$ direction of Ni(111), was significantly modified with respect to bulk Ni. The force constant was in fact 32% softer than the bulk value. This should be referenced to our previous inelastic electron scattering results for Ni(111),[31] which showed Rayleigh wave softening of only 11% along the $\bar{\Gamma}\bar{M}$ direction of Ni(111) as compared to the bulk. These findings stand in sharp contrast to our results for scattering along the direction of the steps, i.e., along the $\bar{\Gamma}\bar{K}$ direction of Ni(111), where no appreciable Rayleigh wave mode softening was observed. These observations effectively rule out the possibility that the softening across the steps is primarily due to step-induced surface interlayer relaxation since such geometry changes (if present) would be expected to affect the surface Rayleigh mode in both directions. The softening could be due to the change in the effective number of nearest neighbor atoms, finite size effects which are present in $\bar{\Gamma}\bar{M}$ direction but are absent in $\bar{\Gamma}\bar{K}$ direction, or intralayer relaxation/stress modification in the direction across the steps. *Ab initio* calculations are clearly needed to assess the actual contributions from different phenomena which lead to this fascinating result. Such calculations are also needed to quantify the extent of charge redistribution near the step edge.

Two new phonon modes were observed in the scattering direction parallel to the steps, i.e., along the $\bar{\Gamma}\bar{K}$ direction of Ni(111). They were definitively assigned as step-edge related modes by observing their strong response to small levels of oxygen adsorption at the steps (they were both quenched while the Rayleigh mode was unaffected), as well as their unusually strong sensitivity to surface temperature. Moreover, their energy dispersion as a function of wave vector clearly differentiated them from the modes found on (smooth) Ni(111). Their polarizations near $\bar{\Gamma}$ were assigned by noting the signal level changes which resulted when we switched from in- to out-of-phase scattering conditions with respect to interferences from the terraces. In the absence of accurate molecular dynamics simulations, we introduced a simple analytic model using a one-dimensional lattice confined by a two-dimensional anisotropic harmonic potential well. From this, we were able to extract effective force constants; $G_1=5.2$ N/m and $G_2=10.4$ N/m for the transverse modes polarized along or perpendicular to the macroscopic surface normal, respectively. Both numbers are much smaller than the bulk single force constant of Ni, 37.9 N/m.[29] This suggests that the effective forces on the step atoms in the direction perpendicular to steps are greatly softened compared to those of the bulk, or even in comparison to the low Miller index surfaces of Ni (low Miller index surfaces are softened 10%–30% compared to the bulk).[29,31] This suggests that the step atoms might be substantially relaxed from the rest of the lattice[16,17] and electronic charge redistribution might be dramatic.[17] *Ab initio* calculations on the Ni(977) surface are again needed to substantiate these effects.

To summarize, inelastic helium scattering has been used to examine the forces present on the terraces and steps of a vicinal metallic surface, Ni(977). Substantial softening has been observed in the terraces in the direction across the step, as well as for the two step-induced transversely polarized vibrational modes that propagate along the step edges. The reduced coordination number for atoms near the step edge plays an obvious and crucial part in these bonding changes. These results point out the importance of understanding how steps modify the electronic charge density distributions (and geometric structure) locally at the steps, as well as in the terraced regions of such interfaces. Information about the forces at the step edges coming from the characterization of these two new phonon modes gives fresh insight into the properties of extended atomic-level surface defects on metallic surfaces, especially how bonding interactions in the vicinity of step edges depart from those characteristic of atomically perfect interfaces. Such findings will be of considerable use in refining our understanding of interface stability, crystal growth, and charge redistribution in the vicinity of extended structural defects on solid surfaces.

ACKNOWLEDGMENTS

We would like to thank Dr. Kevin Gibson and Jennifer Colonell for many helpful suggestions. This work is supported by the Air Force Scientific Research Office and, in part, by the MRSEC Program of the National Science Foundation under Award No. DMR-9400379.

[1] G. A. Somorjai and D. W. Blakely, Nature **258**, 580 (1975).
[2] G. A. Somorjai, in *Advances in Catalysis*, edited by D. D. Eley, H. Pines, and P. B. Weisz (Academic, New York, 1977), pp. 2–66.
[3] S. S. Fu and G. A. Somorjai, Surf. Sci. **262**, 68 (1992).
[4] G. A. Somorjai, Surf. Sci. **299/300**, 849 (1994).
[5] E. D. Williams and N. C. Bartelt, Ultramicrosc. **31**, 36 (1989).
[6] O. L. Alerhand, A. N. Berker, J. D. Joannopoulos, D. Vanderbilt, R. J. Hamers, and J. E. Demuth, Phys. Rev. Lett. **64**, 2406 (1990).
[7] J. J. de Miguel, C. E. Aumann, R. Kariotis, and M. G. Lagally, Phys. Rev. Lett. **67**, 2830 (1991).
[8] C. E. Aumann, J. J. de Miguel, R. Kariotis, and M. G. Lagally, Surf. Sci. **275**, 1 (1992).
[9] T. L. Einstein, T. M. Jung, N. C. Bartelt, E. D. Williams, and C. Rottman, J. Vac. Sci. Technol. A **10**, 1 (1992).
[10] J. Wei, X. S. Wang, J. L. Goldberg, N. C. Bartelt, and E. D. Williams, Phys. Rev. Lett. **68**, 3885 (1992).
[11] T. M. Jung, R. J. Phaneuf, and E. D. Williams, Surf. Sci. **254**, 235 (1991).
[12] N. C. Bartelt, J. L. Goldberg, T. L. Einstein, and E. D. Williams, Surf. Sci. **273**, 252 (1992).
[13] M. B. Webb, F. K. Men, B. S. Swartzentruber, R. Kariotis, and M. G. Lagally, in *Kinetics of Ordering and Growth at Surfaces*, edited by M. G. Lagally (Plenum, New York, 1990).
[14] M. Sokolowski and H. Pfnür, Phys. Rev. Lett. **63**, 183 (1989).
[15] H. Yamaguchi and Y. Horikoshi, Phys. Rev. Lett. **70**, 1299 (1993).
[16] D. L. Adams and C. S. Sorensen, Surf. Sci. **166**, 495 (1986).
[17] J. S. Nelson and P. J. Feibelman, Phys. Rev. Lett. **68**, 2188 (1992).
[18] L. Niu, D. J. Gaspar, and S. J. Sibener, Science (in press).
[19] J. E. Black and P. Bopp, Surf. Sci. **140**, 275 (1984).

Downloaded¬14¬Sep¬2004¬to¬143.106.6.126.¬Redistribution¬subject¬to¬AIP¬license¬or¬copyright,¬see¬http://jcp.aip.org/jcp/copyright.jsp

[20] P. Knipp, Phys. Rev. B **40**, 7993 (1989).
[21] P. Knipp, Phys. Rev. B **43**, 6908 (1991).
[22] R. Berndt, A. Lock, and Ch. Wöll, Surf. Sci. **276**, 213 (1992).
[23] J. E. Black and A. Lock, Surf. Sci. **250**, 279 (1991).
[24] D. D. Koleske, Ph.D. thesis, The University of Chicago, 1992.
[25] H. Ibach and D. Bruchmann, Phys. Rev. Lett. **41**, 958 (1978).
[26] M. Wuttig, C. Oshima, T. Aizawa, R. Souda, S. Otami, and Y. Ishizawa, Surf. Sci. **193**, 180 (1988).
[27] A. Lock, J. P. Toennies, and G. Witte, J. Electron. Spectrosc. Relat. Phenom. **54/55**, 309 (1990).
[28] A. Lock, B. J. Hinch, and J. P. Toennies, in *Kinetics of Ordering and Growth at Surfaces*, edited by M. G. Lagally (Plenum, New York, 1990), p. 77.
[29] S. Lehwald, F. Wolf, H. Ibach, B. M. Hall, and D. L. Mills, Surf. Sci. **192**, 131 (1987).
[30] S. Lehwald, J. M. Szeftel, H. Ibach, T. S. Rahman, and D. L. Mills, Phys. Rev. Lett. **50**, 518 (1983).
[31] W. Menezes, P. Knipp, G. Tisdale, and S. J. Sibener, Phys. Rev. B **41**, 5648 (1990).
[32] B. Gans, S. F. King, P. A. Knipp, D. D. Koleske, and S. J. Sibener, Surf. Sci. **264**, 81 (1992).
[33] M. A. Van Hove and G. A. Somorjai, Surf. Sci. **92**, 489 (1980).
[34] M. J. Stirniman, W. Li, and S. J. Sibener (private communication).
[35] A. J. E. Foreman and W. M. Lomer, Proc. Phys. Soc. London, Sect. B **70**, 1143 (1957).
[36] J. A. Stroscio, M. Persson, C. E. Bartosch, and W. Ho, Phys. Rev. B **33**, 2879 (1986).
[37] M. Persson, J. A. Stroscio, and W. Ho, Phys. Scr. **36**, 548 (1987).
[38] L. Niu, D. D. Koleske, D. Gaspar, S. F. King, and S. J. Sibener (to be submitted).
[39] L. Niu, D. J. Gaspar, and S. J. Sibener (to be submitted).

Downloaded¬14¬Sep¬2004¬to¬143.106.6.126.¬Redistribution¬subject¬to¬AIP¬license¬or¬copyright,¬see¬http://jcp.aip.org/jcp/copyright.jsp